We are IntechOpen, the world's leading publisher of Open Access books Built by scientists, for scientists

4,800
Open access books available

122,000
International authors and editors

135M
Downloads

Our authors are among the

154
Countries delivered to

TOP 1%
most cited scientists

12.2%
Contributors from top 500 universities

CLARIVATE ANALYTICS BOOK CITATION INDEX INDEXED

WEB OF SCIENCE™

Selection of our books indexed in the Book Citation Index in Web of Science™ Core Collection (BKCI)

Interested in publishing with us?
Contact book.department@intechopen.com

Numbers displayed above are based on latest data collected.
For more information visit www.intechopen.com

Chapter 10

Gelcasting of Ferroelectric Ceramics: Doping Effect and Further Development

Dong Guo and Kai Cai

Additional information is available at the end of the chapter

http://dx.doi.org/10.5772/53995

1. Introduction

Ferroelectric ceramics may be seen as the most important type of ferroelectric materials, which have been used in a wide spectrum of electrical and microelectronic devices, including underwater transducers, micro-pumps and valves, ultrasonic motors, thermal sensors, probes for medical imaging and non-destructive testing, and accelerometers, etc (Cross LE, 1996; Setter et al., 2000).

Ferroelectric ceramics used in the devices have various shapes. A certain shape formation technique is required to make ceramics with the desired shapes. Dry pressing is the most commonly used ceramic forming technique. In this technique, dry powders containing organic binder are filled into a solid mold, then dry ceramic green bodies with the shape of the mold cavity are formed under mechanical or hydraulic compacting presses selected for the necessary force and powder fill depth. The pressure is around several tens of MPa or higher. Therefore, large ceramic parts require a much higher compacting force. If the ceramic parts are unable to have pressure transmit suitably for a uniform pressed density then isostatic pressing may be used. One of the most serious disadvantages of dry pressing lies in the difficulty in fabricating high quality large and complex-shaped ceramics or ceramics with a fine structure, which are required for various devices.

To resolve the problems associated with the conventional dry pressing, new wet forming techniques, such as gelcasting (Omatete et al., 1991), electrophoretic casting (Biesheuvel et al., 1999), hydrolysis assisted solidification (Novak et al., 2002), and direct coagulation casting (Graule et al., 1996), etc., are becoming increasingly attractive for advanced ceramic materials. Since in these techniques the ceramic powders are dispersed in a liquid medium and thoroughly mixed, wet forming techniques have the advantages of reducing some structure defects that are difficult to remove in dry pressed ceramic parts. Among the many wet form-

ing techniques, aqueous gelcasting represents the latest improvements. In the technique, a high solids loading slurry obtained by dispersing the ceramic powders in the pre-mixed solution containing monomer and cross-linker is cast in a mold of the desired shape. When heated, the monomer and cross-linker polymerize to form a three-dimensional network structure, thus the slurry is solidified *in situ* and green bodies of the desired shape are obtained, which consists mainly of ceramic powders with a low polymer content. Gelcasting may be seen as a milestone in fabricating complex-shaped ceramic parts since it has initiated a new branch of research in ceramic processing due to its intriguing properties of near-net-shape forming, high green strength, and low binder concentration, etc. As a pressure free method, it can also be used in fabricating large ceramic components that have simple shapes. For example, to make a ceramic disc with a diameter of 20 cm by dry pressing, a load of hundreds of tons is required. In contrast, such a ceramic disc can be easily made by gelcasting via a simple ring-shaped mold at much less cost. Furthermore, gelcasting may be developed to fabricate complex-shaped (Cai et al., 2003) or fine-structured (Guo et al., 2003) ceramic parts that are rather difficult or even impossible to be formed by the conventional dry pressing method.

Since its invention in 1991 gelcasting has been widely used for the fabrication of structural ceramics, including Al_2O_3 (Young et al., 1991), SiC (Zhou et al., 2000), and Si_3N_4 (Huang et al., 2000), etc. Later, it was applied to a number of functional ceramics in a number of ways including $LaGaO_3$ (Zha et al., 2001), ZnO (Bell et al., 2004), and $Sr_{0.5}Ba_{0.5}Nb_2O_6$ (Chen et al., 2006), etc. The first journal report about the application of gelcasting to piezoelectric ceramics appeared at 2002 (Guo et al., 2003). Compared to structural ceramics, much less research about gelcasting of functional ceramics has been conducted so far.

Among the many ferroelectric ceramic materials, lead zirconate titanate (PZT) is the most widely used one owing to their superior piezoelectric, pyroelectric and dielectric properties. A fascinating feature of multicomponent ferroelectric ceramics is that their electrical properties can be modified by doping with acceptors and donors (Shaw et al., 2000). As a result, a series of PZT materials with tailored properties are commercially available. Unfortunately, this feature also leads to the problem of high sensitivity of the electrical properties of PZT to composition. In addition, PZT is commonly used with a composition close to the morphotropic phase boundary (MPB) at a Zr/Ti ratio of about 52/48, where properties such as piezoelectric coefficients, dielectric permittivity, and coupling factors are maximized and thus may be more sensitive to the composition (Noheda et al., 2006). On the other hand, since shape formation in gelcasting is achieved through *in situ* polymerization, organic additives are used in the premix solution. Also, addition of commercial surfactants that may have a complicated composition is indispensable, because successful fabrication of ceramics via gelcasting or other colloidal methods requires to prepare high solids loading ceramic slurry with still a low viscosity. Consequently, in order to apply gelcasting to the formation of ferroelectric ceramics such as PZT, it is necessary to remove the possible influence of the impurities introduced by the various additives on the electrical performance of the final products. This makes the problems more complicated than that of structural ceramics.

http://dx.doi.org/10.5772/53995

2. Colloidal chemistry and rheological properties of PZT suspensions

We first give a short introduction the gelcasting technique. The details are out of the focus of this chapter, and interested readers can refer to other papers. According to the liquid medium used, there are two types of gelcasting systems: aqueous and nonaqueous systems. In aqueous gelcasting deionized water is used as the medium, and acrylamide ($C_2H_3CONH_2$) may be seen as a prototype monomer. Generally, N,N-methylenebisacrylamide ($(C_2H_3CONH)_2CH_2$, MBAM) N,N,N_0,N_0-Tetramethylethylenediamine (TEMED) and $(NH_4)_2S_2O_8$ are used as the cross-linker, the catalyst and the initiator, respectively. The gelcasting process of PZT is similar to that of previous studies. The flowchart of the gelcasting is shown in Figure 1. First, the PZT powders are added in the premix solution containing AM and MBAM and thoroughly mixed. After addition of initiator and catalyst, the slurry is de-aired in vacuum, then the slurry is cast into the mold with desired shape and heated around 60-80°C in a oven for several hours for polymerizatoin and drying. After demolding the green ceramic body is obtained.

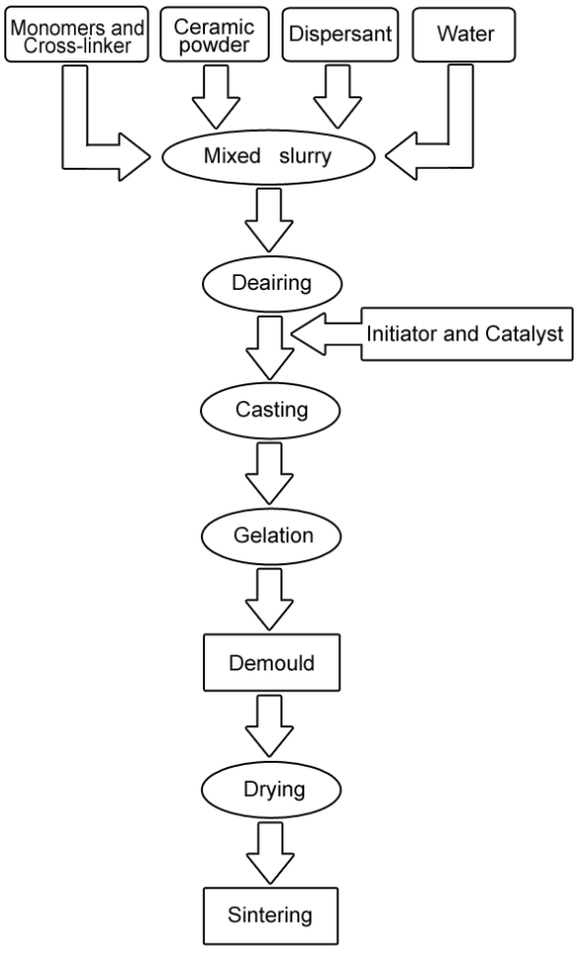

Figure 1. The flowchart of gelcasting

The colloidal and rheological properties of the PZT suspension are important issues that should be addressed first. Homogenous dispersion of the powder in the premix solution and stability of the suspension are determined mainly by attractive and repulsive forces between the particles in the system. The former generally arises from the van der Waals forces while the latter can arise from electrostatic repulsion or steric repulsion of surfactant materials absorbed on the particle surfaces (Israelachvili, 1992). Magnitude of the van der Waals forces is mainly determined by the nature of the particle surface and the solvent. While the repulsive forces can be modified over a wide range by dispersants.

Commercial Name	**TAC**	**JN281**	**SP2**	**SGA**
Producer	Beijing Chemical Reagent Co.	Beijing Pinbao Chemical Co.	Beijing Tongfang Chemical Co.	Beijing Tongfang Chemical Co.
Composition	Triammonium citrate	Poly (acrylic acid), NH_4^+ salt solution	Poly (acrylic acid-co-maleic acid), Na^+ salt solution	Poly (acrylic acid), Na^+ salt solution

Table 1. Composition and producer of the dispersants

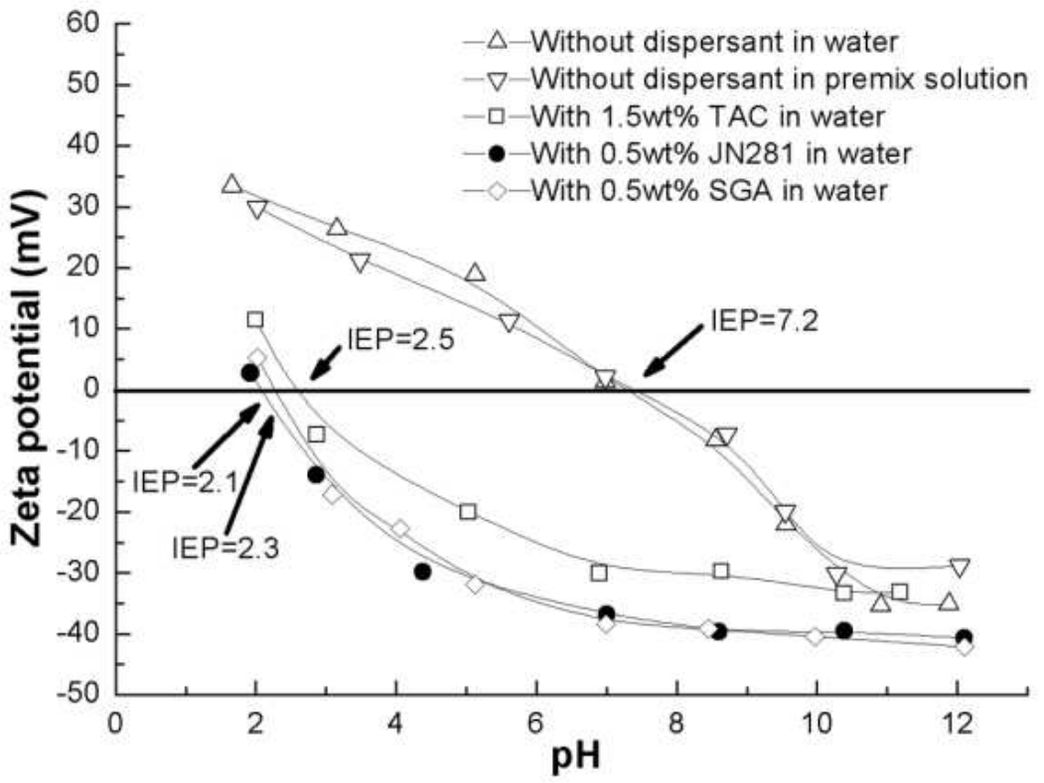

Figure 2. Effect of dispersants on the zeta potentials of the PZT suspensions at different pH values.

Polyelectrolyte dispersants are well known to be effective for various ceramic slurries due to both electrostatic and steric repulsions of the macromolecules. Here we show the effects of

http://dx.doi.org/10.5772/53995

typical polyelectrolyte dispersants and a widely used organic surfactant triammonium citrate (TAC). The details are listed in Table 1. Electrostatic repulsion is dependent on the zeta potential (ζ) of the powders. The higher this value with the same polarity, the stronger the electrostatic repulsion between the particles. When close to the isoelectric point (IEP), the particles tend to flocculate. Zeta potentials of various PZT aqueous suspensions (0.06 vol % solids) at different pH values are shown in Figure 2. The zeta potential of pure PZT suspension changes from 33 mV at pH = 1.7 to - 35.1 mV at pH = 11.9 with an IEP at about pH = 7.2, suggesting that neutral environment is disadvantageous for good dispersion. Addition of monomer only slightly decreases the relative value of the potential and has little effect on IEP, indicating that the uncharged AM molecules screen the charge of the PZT particles. With the addition of TAC, JN281 and SGA the IEP is moved to pH = 2.5, 2.1 and 2.3, respectively. In the range of neutral environment to pH = 12, the zeta potential is almost constant. The higher absolute potential values of suspensions with JN281 and SGA than that with TAC imply that polyelectrolyte dispersants are more effective as far as the electrostatic repulsion is concerned.

Figure 3 shows the viscosity as a function of the shear rate for different PZT slurries solids loading. Adjustment of pH values to either acid or basic conditions has little effect, while addition of dispersants can greatly decrease the viscosity. The high viscosities at the beginning indicate a 'Bingham' type behavior, which is followed by a shear thinning at low shear rates. Shear-thinning behavior can be attributed to a certain kind of rearrangement of the relative spatial disposition of the particles. For concentrated suspensions of hard solid particles in Newtonian liquids, a flow-induced layered structure has been verified (Ackerson, 1990). Such a structure can provide a low resistance of the particle movement between different layers under the shear flow. For the systems containing dispersants, when the shear rates increase to a critical value (γ_c) a shear-thickening behavior appears, indicating that the flow-induced structure is destroyed. It is clear that the polyelectrolyte dispersants are much more effective than TAC. In addition, PZT slurries in the premix solution have almost the same viscosity values as those in the pure water, suggesting that addition of AM (15 wt.%) has little effect on the viscosity. These and the zeta potential results indicate that the polyelectrolyte dispersants work by both electrostatic and steric stabilization mechanism.

Generally, there is a complex nonlinear relationship between viscosity and solids volume fraction, which is closely related to many factors, including the continuous phase viscosity, particle-size distribution, and particle shape, etc. Influence of solids loading on the apparent viscosity is shown in Figure 4. At low solids loading the slurries show a low viscosity. The continuous addition of particles finally three-dimensional contact throughout the suspension, making flow impossible. The particular solid phase volume at which this happens is called the maximum packing fraction Φ_m (Barnes & Hutton, 1989). Before adding dispersant the PZT suspension has a measurable viscosity at a solids loading slightly smaller than 32 vol.%. Adding a little more PZT powders leads to a 'solidified' slurry whose viscosity is impossible to be measured by the normal rheometer. The Φ_m is thus determined to be 32 vol.%. Adding 0.8 and 1.5 wt.% of TAC increase Φ_m to about 47 and 53 vol.%, respectively. The lower Φ_m for a TAC concentration of 2.2 wt.% indicates that excess dispersant is harmful.

The relationship between the viscosity and the solids volume fraction for monodispersed suspension can be explained by the Krieger–Dougherty (K–D) model:

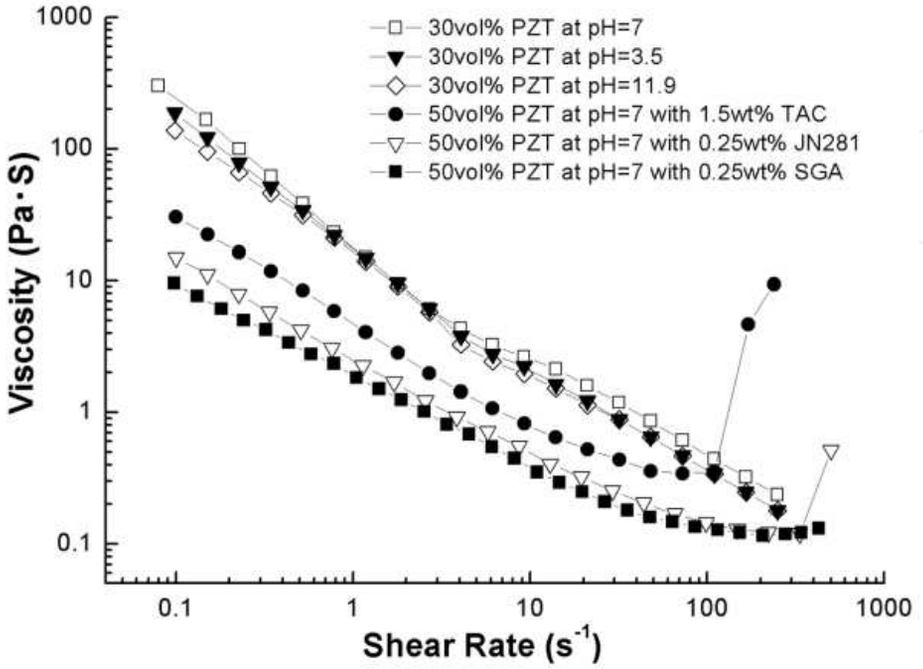

Figure 3. Influence of dispersants and pH value on the viscosity of the PZT suspensions

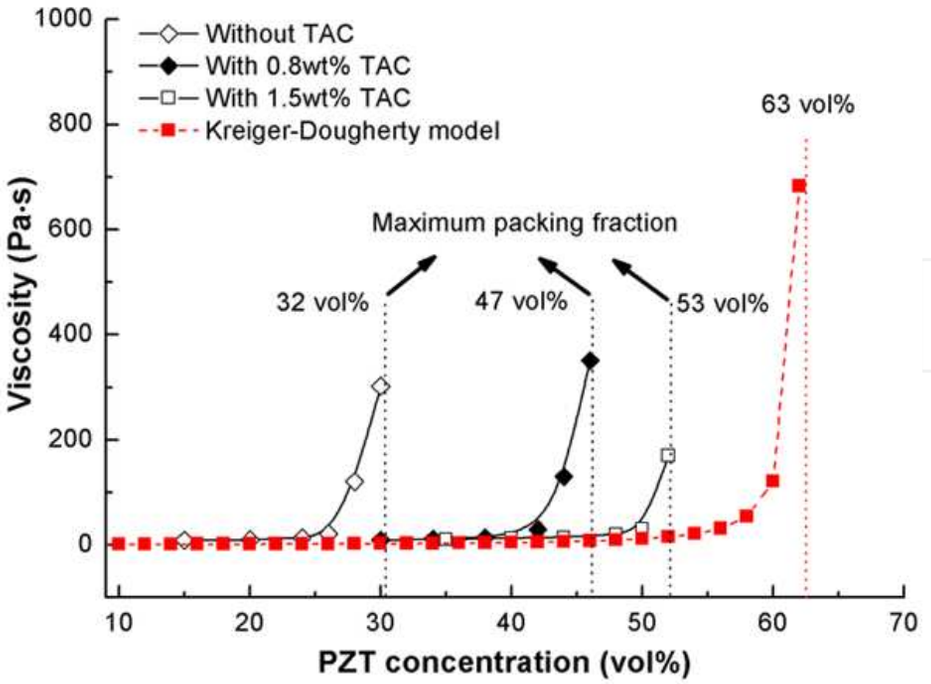

Figure 4. Influence of solids loading on the viscosities of the PZT suspensions

http://dx.doi.org/10.5772/53995

$$\eta = \eta_o(1-\phi/\phi)^{-[\eta]\phi_m} \quad (1)$$

where η and η_o are the viscosity of the suspension and the solvent, respectively. The true volume fraction of the powder in the suspension is represented by f. The intrinsic viscosity [η] is a function of particle geometry; a value of 2.5 is suitable for spherical particles. A maximum packing fraction of 0.63±0.002 is suitable for random close packing at low shear rate. The K–D model curve with [η] = 2.5 and Φ_m=0.63 is plotted in the Figure. Although the experimental curves are somewhat deviated from the K–D model, they still show a similar shape: low viscosity at low solids loading and sharp increase at high solids loading. The discrepancy may partly be ascribed to the inhomogeneity of the particle size. In addition, particle flocculation will lead to a lower Φ_m because the flocs themselves are not close-packed (Starov et al., 2002) and they can trap part of the liquid phase, thus, leading to higher 'effective phase volume' and viscosity than those of the primary particles. The results clearly show the remarkable effect of dispersants in getting low viscosity ceramic slurry.

3. Electrical characterization and analysis of the doping effects

3.1. Electrical characterization for identifying the doping type

The piezoelectricity of PZT type materials originates from the displacement of Zr and Ti sublattices and the electrical properties of the materials can be dramastically affected by doping atoms. There are primarily two types of dopants for PZT, i.e. the donor type (soft type), and the acceptor type (hard type) (Jaffe et al., 1971). The former is mainly caused by substitution of higher valence ions for the A site Pb or B site Zr and Ti, and correspondingly higher piezoelectric coefficient (d_{33}), planar electromechanical coupling factor (K_p), relative permittivity (ε_r), loss tangent ($tg\delta$), P_r values and a lower mechanical quality factor (Q_m) value are obtained. The latter, which is caused by substitution of lower valence ions for the A or B site atoms, has contrary effects.

Sample	Average d_{33}	ε_r	tgδ	K_P
Dry pressed	469 pC/N	1430	0.0311	0.621
G-TAC	468 pC/N	1369	0.0325	0.633
G-JN281	479 pC/N	1352	0.0401	0.675
G-SP2	403 pC/N	1285	0.0250	0.591
G-SGA	330 pC/N	1244	0.0202	0.541

Table 2. Comparison of densities and some electrical parameters of dry pressed and gelcast PZT samples.

Some electrical parameters of different soft-doped PZT samples are compared in Table 2, where G-TAC, G-JN281, G-SP2 and G-SGA represent the best available gelcast PZT samples with TAC, JN281, SP2 and SGA as the dispersants, respectively. The ε and $tg\delta$ are 1 kHz data under room temperature. The dry pressed sample is obtained under a pressure of ~ 80MPa. G-TAC shows similar electrical properties with those of the dry pressed one. This indicates that the organic species used in gelcasting, including the dispersant TAC, the monomer and the cross-linker, etc., have almost no doping effects. Compared to the dry pressed sample, G-SP2 and G-SGA show higher Q_m and decreased d_{33}, K_p, ε, $tg\delta$ and P_r values, while change of these parameters for G-JN281 is to the contrary. Thus, the data in reveal that SP2 and SGA induced evident 'hard' doped characteristics, while JN281 induced 'soft' doped characteristics. Except for the dispersant species, the samples were prepared under the same conditions. Hence, the different properties should be mainly attributed to the dispersants used. A 'fingerpint' of hard doping effect is the increased Q_m (Damjanovic, 1998). Since Na^+ is the main metal cation in SP2 and SGA, we neglect other difference and check the correlation between Na concentration (inspected by X-ray Fluorescence) and Q_m. As shown in Figure 5, Q_m roughly shows an increasing trend with Na mole fraction except for G-JN281. Then we intentionally introduced Na into the G-JN281 by adding NaOH to the corresponding slurry to increase its pH value to ~13. As expected, a higher Q_m is indeed obtained after adding Na to G-JN281. These reveal that the Na^+ ion introduced by the dispersants has a stronge doping effect for gelcast PZT. From the valence and diameter (1.02Å) of Na^+, we deduce that it should substitute for the A site Pb^{2+} (1.18Å) as an acceptor dopant.

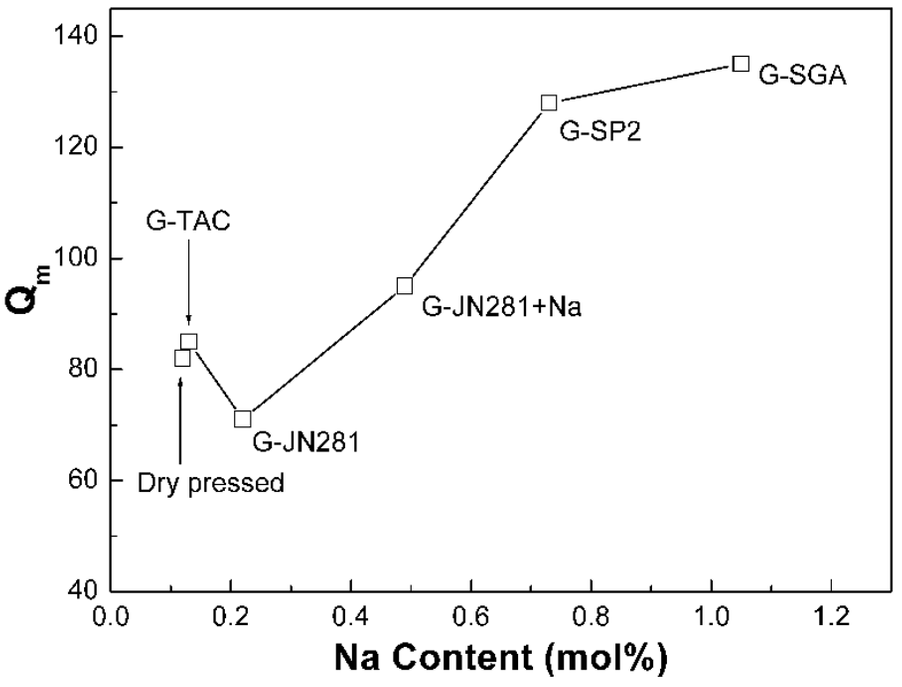

Figure 5. Illustration of the relationship between Na concentration (mole percentage in total metal elements) and Q_m of various PZT samples.

http://dx.doi.org/10.5772/53995

3.2. Complex impedance spectra

Figure 6(a), 6(b), 6(c) and 6(d) show the complex impedance spectra in the temperature range of 300~540 °C of the dry pressed sample, G-JN281, G-JN281+Na and G-SP2, respectively. The spectra of G-TAC is very similar with those of the dry pressed sample and thus not shown. The complex impedance spectra of all samples show only one Cole-Cole semicircle crossing the origin, which can be assigned with an equivalent circuit composed of a simple parallel RC element with a impedance that can be expressed as equation (2):

$$Z = \frac{R}{1 + (i\omega RC)^{1-n}}, \tag{2}$$

where the parameter n characterizes the distribution width of the relaxation times around a mean value τ_0=RC (West et al., 1997). The semicircles of the samples show no obvious depression, i.e. the depression angle β (=nπ/2) between the real axis and the line from the high frequency intercept to the centre of the circle is close to 0. Thus, n is close to 0, indicating a debye-like behavior with a single relaxation time (West, 1997; Cao, 1990). Then based on equation (2) the following relationship about the real (Z′) and imaginary (Z″) parts of the impedance can be derived:

$$\left(Z' - \mathrm{R}/2\right)^2 + Z''^2 = \left(\mathrm{R}/2\right)^2. \tag{3}$$

The resistance R derived from the diameter of the semicircle, and the capacitance C can be derived from the angular frequency ω at the peak of the circular arc based on the relationship ωRC=1. The C values of the samples are in the order of 10^{-10}-10^{-9} F, which can be associated with the intrinsic ferroelectric bulk (or grain) response.

Using the R values, the logarithm of conductivity of different samples as a function of reciprocal temperature is plotted in Figure 6(e). The conductivity σ of the ferroelectric bulk phase shows an Arrhenius type behavior that can be described by equation (4):

$$\sigma = \sigma_o \exp(\frac{-E_s}{kT}), \tag{4}$$

where σ_0, E_g, k and T are the pre-exponential factor, the activation energy, the Boltzmann's constant and the absolute temperature, respectively. The logarithm of equation (4) gives equation (5):

$$\ln\sigma_T = \ln\sigma_o - \frac{E_s}{k}(\frac{1}{T}) = -2.30259 \log \rho_{T,} \tag{5}$$

where ρ_T is the resistivity. Based on the sample geometry, the E_g values associated with the intrinsic bulk phase conduction of the samples were derived by using equation (5). The data are compared in Table 3.

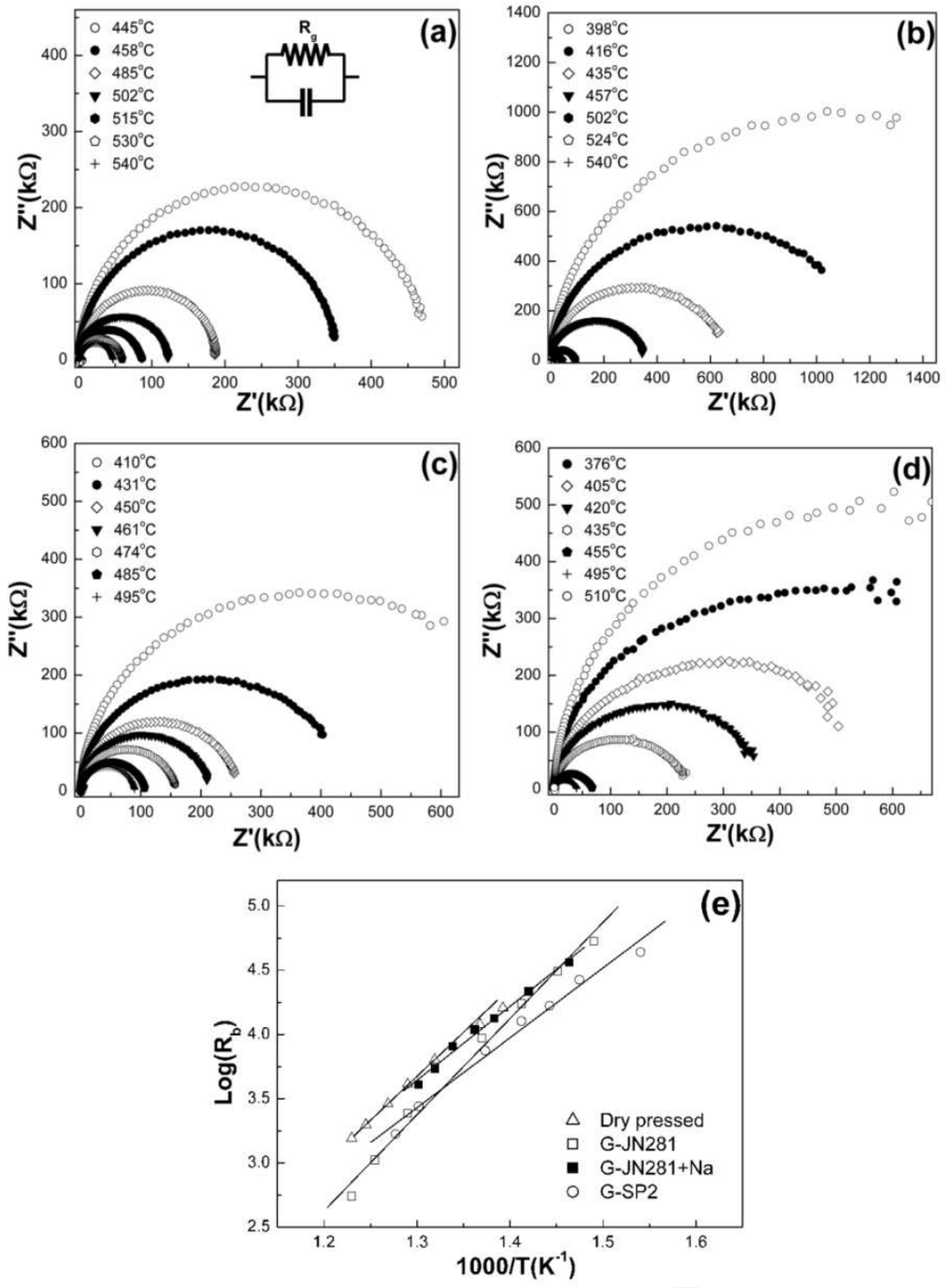

Figure 6. Complex impedance spectra of different PZT samples. (a) Dry pressed. (b). G-JN281. (c) G-JN281+Na. (d) G-SP2. (e) Arrhenius plot for the ferroelectric bulk resistivity of the samples derived from the impedance spectra.

Sample	Dry pressed	G-JN281	G-JN281+Na	G-SP2	G-SGA
E_g	1.24 eV	1.48 eV	1.14 eV	1.08 eV	1.07 eV

Table 3. Comparison of the conductivity activation energies of different PZT samples.

http://dx.doi.org/10.5772/53995

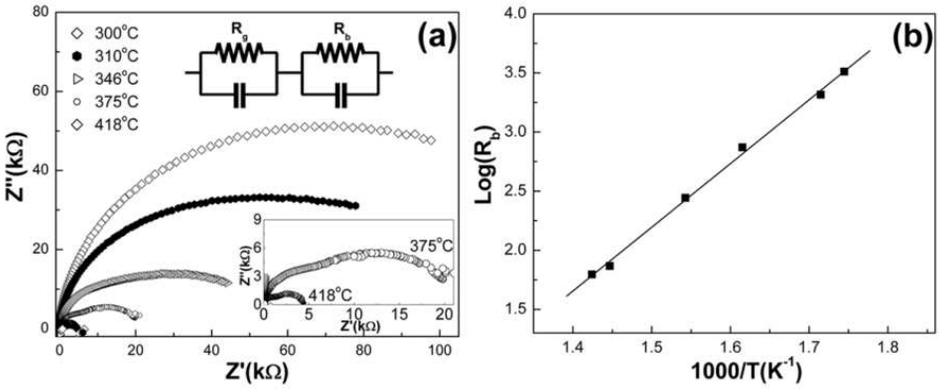

Figure 7. (a) Complex impedance spectra of G-SGA. The inset shows the magnified 375$_o$C and 418$_o$C curves. (b) Arrhenius plot of the ferroelectric bulk phase resistivity of the sample derived from the grain response of its impedance spectra.

The spectra of G-SGA shown in Figure 7(a), particularly the high temperature curves shown in the inset, consist of two semicircles, which can be assigned with an equivalent circuit composed of two parallel RC elements. This indicates the much different 'electrical microstructure'[14] of G-SGA, which has the highest Na concentration. The capacitance obtained by fitting the first semicircle can also be attributed to the ferroelectric bulk response, while the second semicircle may be attributed to the grain boundary response due to the higher capacitance. Actually, one semicircle spectrum may also appear if different responses in a sample overlap as a result of their similar relaxation time. A closer check of Figure 6(d) indicates that the one semicircle impedance spectra of G-SP2 have a slightly higher depression angle than other spectra in Figure 6, consistent with its higher Na concentration (see Figure 5). These imply that the grain boundary response is gradually magnified with increasing Na concentration. The Arrhenius plot of the conductivity of the bulk phase response of G-SGA is shown in Figure 7 (b). The derived E_g value is also listed in Table 3.

The loss of PbO through its volatility causes oxygen vacancies in PZT, leading to a p-type conductivity (Barranco et al., 1999). The acceptor Na^+ incorporated by the dispersants can substitute for Pb^{2+}, which can be expressed as following:

$$Na_2O=2Na_{pb}'+O_o+V_o \quad (6)$$

Thus, Na^+ ions replace Pb^{2+} ions and more oxygen vacancies are simultaneously created for charge compensation. Oxygen vacancies are the only lattice defects in the perovskite oxides that have a significant mobility, and the conductivity should be improved by the oxygen vacancy conduction mechanism via hopping of atoms in the oxygen octahedral network (Raymond & Smyth, 1996). This well explains the lower E_g data of G-SP2 and G-SGA than that of the dry pressed sample (Table 3), revealing again the hard doping effect of the Na-containing dispersants. The relatively higher activation energy of G-JN281 implies the presence of a certain donor-type impurity in G-JN281. Addition of NaOH into G-JN281 leads to a lower E_g value and further confirms the doping effect of Na.

3.3. Ferroelectric hysteresis loops

The ferroelectric (polarization-electric field) hysteresis loops of the PZT samples are shown in Figure 8. In Figure 8(a), G-SP2 and G-SGA show remnant polarization (P_r) of 32.7 μC/cm^2 and 16.7 μC/cm^2, respectively. Both values are smaller than the value of 39.8 μC/cm^2 of the dry pressed sample. The difference can also be interpreted by increased oxygen vacancies due to doping of Na. As afore mentioned, oxygen vacancies can move in the oxygen octahedral network. This may lead to a low stability of the $2Na_{pb}'$-V_o defect dipoles. The defect dipoles tend to orient themselves along the polarization direction, resulting in stabilized ferroelectric domains. A stabilized domain wall structure in turn give rise to more difficult poling and depoling (switching) and a smaller P_r (Warren, et al., 1996; Lambeck & Jonker, 1978). The round open loop of G-SP2 implies a higher leakage current. The hysteresis loops of G-JN281 and G-JN281+Na in Figure 8 (b) also clearly demonstrates the effect of Na: decreased P_r and a loop with a rounder shape.

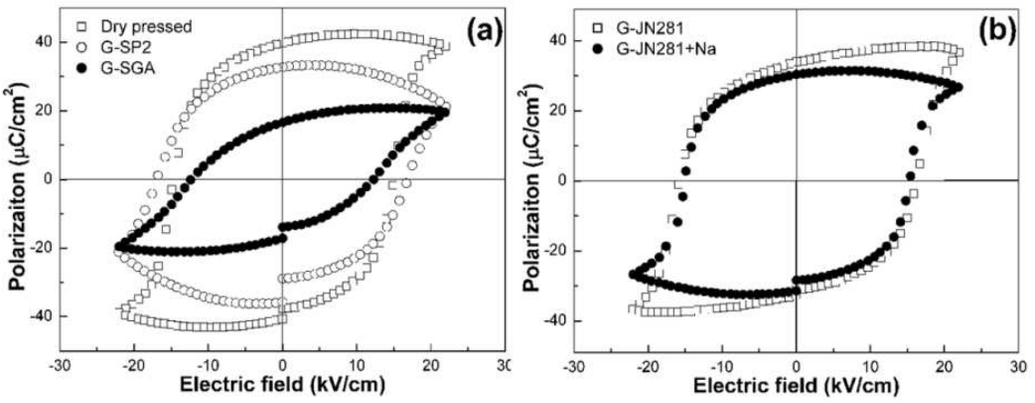

Figure 8. Ferroelectric hysteresis loops of the PZT samples.

4. Microstructural characterization

The XRD spectra of All samples (Figure 9) show typical perovskite structures (Soares et al., 2000; Hammer et al., 1998). The XRD patterns of G-TAC, G-SP2 and G-SGA are very similar to that of the dry pressed sample. While the peaks of the XRD pattern of G-JN281 shift very slightly to higher diffraction angles, indicating a contracted lattice cell. Considering the soft doped characteristics of G-JN281, the change in its XRD pattern may again be attributed to a certain unknown donor impurity ion introduced by the dispersant.

http://dx.doi.org/10.5772/53995

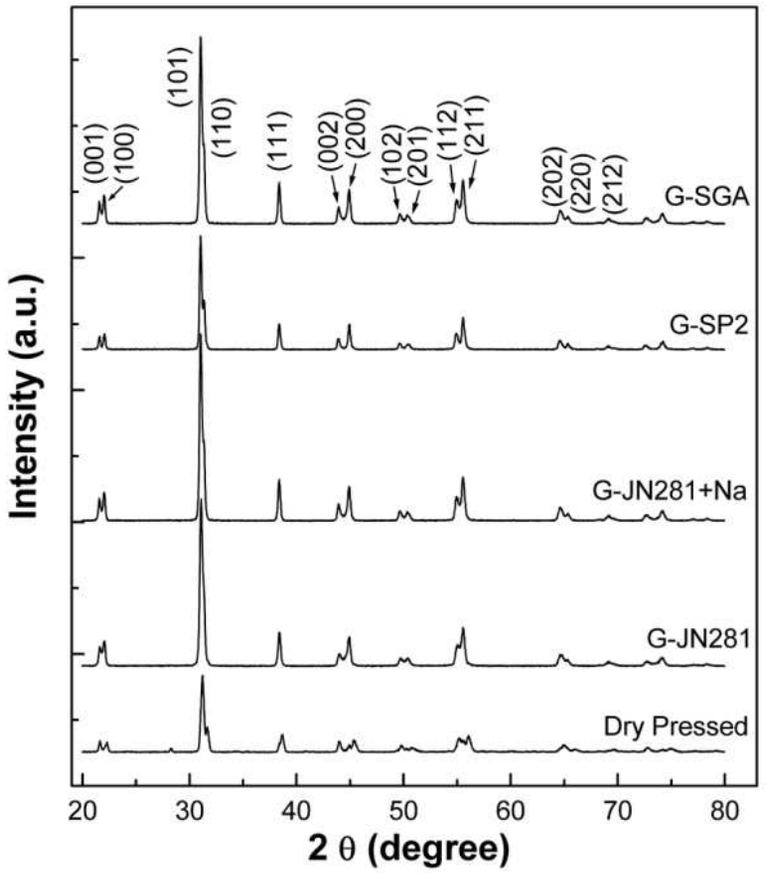

Figure 9. XRD patterns of different PZT samples.

As shown in Figure 10, although sintered under the same procedure, the samples exhibit rather different morphologies. SEM image of G-JN281+Na is not illustrated since it is very similar to that of G-JN281. Dry pressed sample shows an intergranular fracture surface and relative uniform grains with a diameter of 3~5 μm. G-JN281 shows a morphology very similar to that of the dry pressed one. G-SP2 also shows a basically intergranular fracture surface, but the grains are much larger with a diameter of 6~10 μm. Much different from other samples, G-SGA shows a transgranular fracture surface with the largest grains with a diameter of about 12 μm. Such a transgranular growth may result from chemical inhomogeneity and presence of intergranular phases or expanded grain boundary region. This is consistent with the two semicircle impedance spectra of G-SGA shown in Figure 7 (a).

In summary, electrical and structural characterization indicate that the Na^+ ion, which is the main cation in many widely used commercial dispersants (Xu et al., 1996; Tomasik et al., 2003), shows detrimental hard doping effects, leading to deteriorated electrical performance. Also, the impurity species introduced by dispersants or other additives may have a complicated influence on the electrical properties and microstructure of gelcast PZT samples. The results indicate that the specific doping effect, e.g. the change in electrical performance by the additives during processing, is a critical issue that should be paid special attention when applying gelcasting to the formation of electronic ceramics.

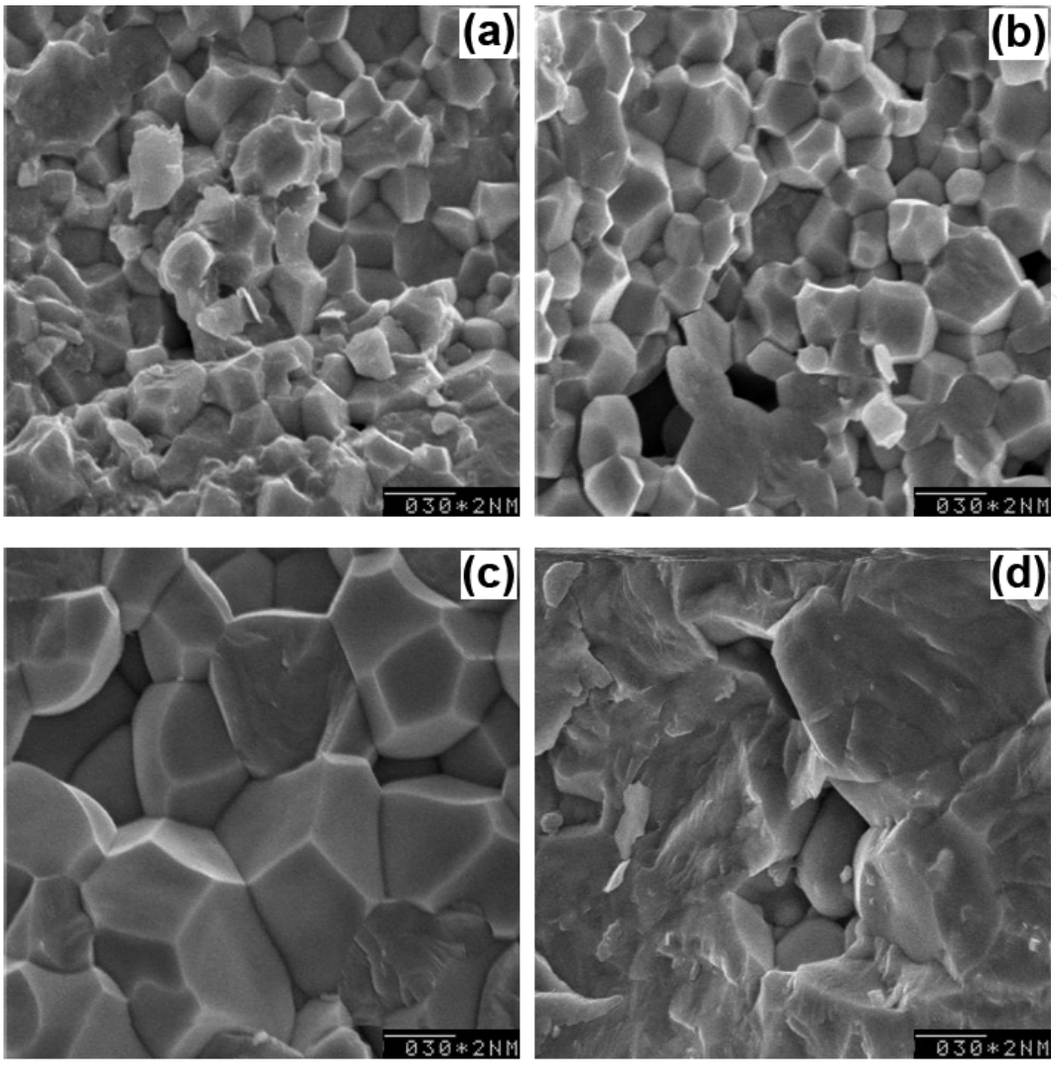

Figure 10. SEM images of the fracture surfaces of different PZT samples. (a) Dry pressed sample; (b) G-JN281; (c) G-SP2; (d) G-SGA.

5. Development of gelcasting for special-shaped PZT ceramics

Application of gelcasting to ferroelectric ceramics is not a mechanical copy of the technique to a different powder material. In addition to the demonstrated doping effect of the necessary additives, there are many other specific issues deserving further investigation. The many devices require the ferroelectric ceramic components to have various specific shapes (Scott, 2007). The shapes of the gelcast bodies are formed during gelation and drying process with the confinement of the molds. The two most critical issues about shape formation that have attracted more and more attention are probably the fracture (or crack growth) and deformation of the ceramics. No doubt that the former should be avoided, however, what is interesting is that the latter may even be used to form shapes that are difficult to formed by the molds. The two issues are briefly discussed in the following.

http://dx.doi.org/10.5772/53995

5.1. Factors affecting fracture and crack growth

Fracture or crack growth results from the competition of the strength of the gelcast body and the stress developed during gelation and drying. Many factors can affect fracture or crack growth, including the monomer concentration, monomer/cross-linker ratio, initiator concentration, initiator/catalyst ratio, gelation temperature and drying condition (humidity), etc (Ma et al., 2006). It is easy to be understood that too low a monomer concentration is insufficient to keep the three dimensional polymer network structure. A suitable monomer/cross-linker ratio is necessary to keep a strong gelcast body with still controllable stresses. Compared to other factors, initiator and catalyst seem to be more critical in controlling the gelcast body strength and stresses, since they can determine the 'joints' of the gel network. As shown in Figure 11. A slight decrease of the $(NH_4)_2S_2O_8$ concentration from the normal level causes a seriously broken green body. In addition to use of optimized premix solution, drying is a complicated process that should be carried out under contolled humidity (Barati et al., 2003).

Fracture or crack growth may also appear after sintering (Zheng et al., 2008), even if the shapes of the ceramics are well preserved after drying. During sintering the macromolecular gel network is destroyed and the stresses developed due to material densification may give rise to fracture or cracks in the ceramic body with decreased strength.

Figure 11. A fractured PZT-4 type green body caused by a lower initiator concentration

5.2. Deformation controllable gelcasting

Factors that affect crack growth discussed in the forgoing section also affect deformation. In most cases, deformation should be kept as smaller as possible. However, well controlled deformation can also be used to fabricate certain devices that use specially-shaped PZT as the active components. Here we show two examples: spherical PZT shell vibrator and PZT minitube.

As an effective non-invasive surgical tool, High intensity Focused sound (HIFU) has been used for the treatment of human tissues such as liver, kidney, breast, uterus and pancreas, and it is receiving growing interest (Wan, et al., 2008; Davies et al., 1998). As shown in Figure 12, some therapeutic HIFU transducers require to use spherical piezoelectric PZT shells as the active components (Saletes et al., 2011). Conventionally, such a spherical plate is fabricated by grinding both sides of a cylindrical plate. The mechanical method is time-consuming and wastes a lot of PZT material. Gelcasting of flat PZT plates generally uses a cylindrical ring mold and a flat bottom plate. During drying, the upper surface of the gelcast body is exposed to atmosphere while the other side is still berried until the whole body solidifies. Then we found an interesting phenomenon: the upper part of the gelcast body might dry and shrink first and a spherical plate was formed. By using suitable premix solution and under well controlled temperature and humidity, the plate edge bends up and a rather ideal spherically shaped PZT green plate can be formed. After sintering a spherical PZT plate was formed, which only needs to be grinded slightly to produce a homogenous spherical vibrator. Furthermore, because a lower humidity and a higher temperature can give rise to a larger deformation, the curvature radius can be controlled in a certain range under well controlled experimental conditions. So far the smallest focal length obtained for a plate with a diameter of 10 cm without further machining is around 15 cm. A PZT-8 plate with a diameter of 12 cm is shown in Figure 13.

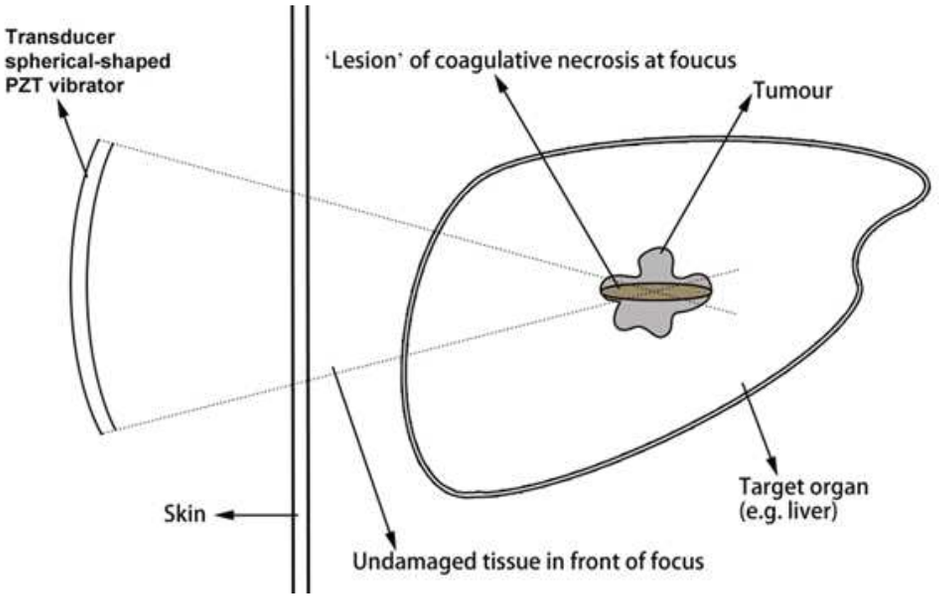

Figure 12. Schematic illustration of the therapeutic effect of a HIFU transducer

http://dx.doi.org/10.5772/53995

5.3. Fabrication of hollow spherical PZT shell

Thin-walled hollow sphere Omnidirectional Transducer has been used in hydrophones for many years (Li et al., 2010), which uses a hollow spherical PZT shell as the active component. Hollow spherical PZT shell is generally fabricated by Cold isostatic pressing, which requires complicated facilities. We show here that gelcasting can be developed to fabricate such Hollow spherical PZT shells by using a ball-shaped removable polymeric mold. First, the polymeric ball mold is fixed in a normal metal mold with a large spherical cavity, then the aqueous PZT premix slurry is poured into the mold. After gelation and drying, the whole mold containing the PZT green body and polymeric ball is removed by a careful thermal treatment. The most critical step in this method is thermal treatment, which solidifies the PZT slurry and melt the polymeric ball in due time. A PZT-4 hollow spherical shell with a focal length of ~ 200 mm, a diameter of ~ 120 mm and a wall thickness of 2 mm is also show in Figure 13.

Figure 13. Illustration of special-shaped gelcast PZT ceramics: spherical PZT plate and hollow spherical PZT shell.

In addition to the above mentioned advanced techniques, other gelcasting based ceramic fabrication or processing techniques have been developed in the authors' group, including spatter laser drilling techniques (Guo, 2004), and Rapid Prototyping of PZT bodies by combining gelcasting and Selective Laser Sintering (Guo, 2003), etc.

6. Conclusions

Comparison of various electrical properties and microstructures of various gelcast soft PZT samples with those of the dry pressed PZT one suggests that the Na^+ ion, which is the main cation in many widely used commercial dispersants, shows detrimental hard doping effects, leading to deteriorated electrical performance. The conclusion may be transferable to other doping ions like K^+, which is also contained in many commercial dispersants. Also due to the doping ions introduced by dispersants, the performance of the glecast PZT sample may

also be improved as well. Considering that dispersants are indispensible in getting concentrated low viscosity ceramic slurries, the possible doping effect of metal ions or impurities introduced by the dispersants or other additives should be generally considered when applying gelcasting to forming multicomponent electronic ceramic materials whose electrical properties are sensitive to the composition.

In addition, we also demonstrate some advanced gelcasting techniques, including deformation controllable gelcasting of spherical PZT disc and gelcasting based hollow spherical PZT fabrication technique, etc. Application of gelcasting to PZT is not a mechanical copy of the technique to a different powder material. The results show that successful application of gelcasting to ferroelectric ceramics is not a mechanical copy of the technique to a different powder material.

Author details

Dong Guo[1] and Kai Cai[2]

1 Institute of Acoustics, Chinese Academy of Sciences, Beijing, China

2 Beijing Center for Chemical and Physical Analysis, Beijing Municipal Science and Technology Research Institute, Beijing, China

References

[1] Crsos, LE. (1996). Ferroelectric materials for electromechanical transducer applications. *Materials Chemistry and Physics*, 43, 108-115

[2] Setter, N.; Waser, R. (2000). Electroceramic materials. *Acta Materialia*, 48, 151-178

[3] Omatete, O.O.; Janney, M.A.; Strehlow, R.A. (1991). Gelcasting: a new ceramic forming process. *American Ceramic Society Bulletin*, 70, 1641-1649

[4] Biesheuvel, PM.; Verweij, H. (1999). Theory of Cast Formation in Electrophoretic Deposition. *Journal of the Amarican Ceramic Society*, 82, 1451-1455

[5] Novak, S.; Kosmac, T.; Krnel, K.; Drazic, G. (2002). Principles of the hydrolysis assisted solidification (HAS) process for forming ceramic bodies from aqueous suspension. *Journal of the European Ceramic Society*, 22, 289-295

[6] Graule, TJ.; Gauckler, LJ.; Baader, FH. (1996). Direct coagulation casting–a new green shaping technique.PT.1. processing principles. *Industrial Ceramics*, 16, 31-34

[7] Cai, K.; Guo, D.; Huang, Y.; Yang, JL. (2003). Solid freeform fabrication of alumina ceramic parts through a lost mould method. *Journal of the European Ceramic Society*, 23, 921-925

[8] Guo, D.; Li, LT.; Gui, ZL.; Nan, CW. (2003). B-Solid state materials for advanced technology. *Materials Science and Engineering*, 99, 25-28

[9] Young, A.C.; Omatete, O.O.; Janney, M. A.; Menchhofer, P.A.(1991). Gelcasting of Alumina. *Am.Ceram. Soc*, 74, 612-618

[10] Zhou, LJ.; Huang, Y.; Xie, ZP.; (2000). Gelcasting of concentrated aqueous silicon carbide suspension. *Journal of the European Ceramic Society*, 20, 85-90

[11] Huang, Y.; Ma, LG.; Tang, Q.; Yang, JL.; Xie, ZP.; Xu, XL. (2000). Surface oxidation to improve water-based gelcasting of silicon nitride. *Journal of Materials Science*, 35, 3519-3524

[12] Zha, SW.; Xia, CR.; Fang, XH.; Wang, HB.; Peng, DK.; Meng, GY. (2001). Processing and electrical properties of doped-$LaGaO_3$ by gelcasting. *Ceramics Intrernational*, 27, 649-654

[13] Bell, NS.; Voigt, JA.; Tuttle, BA. (2004). Colloidal processing of chemically prepared zinc oxide varistors. Part II: Near-net-shape forming and fired electrical properties. *Journal of Materials Research*, 19, 1341-1347

[14] Chen, W.; Kinemuchi, Y.; Watari, K.; Tamura, T.; Miwa, K. (2006). Preparation of Grain-Oriented $Sr_{0.5}Ba_{0.5}Nb_2O_6$ Ferroelectric Ceramics by Magnetic Alignment. *Journal o f the American Ceramic Society* , 89, 381-384

[15] Guo, D.; Cai, K.; Li, LT.; Gui, ZL. (2003). Application of gelcasting to the fabrication of piezoelectric ceramic parts. *Journal of the European Ceramic Society*, 23, 1131-1137

[16] Shaw, TM.; Trolier-McKinstry, S; McIntyre, PC.; (2000). The Properties of Ferroelectric Films at small dimensions. *Annual Review of Materials Science*, 30, 263-298

[17] Noheda, B.; Cox, DE. (2006). Bridging phases at the morphotropic boundaries of lead oxide solid solutions. *Phase Transitions*, 79, 5-20

[18] Israelachvili, J.; (1992). *Intermolecular & Surface Forces, 2nd ed.*

[19] Ackerson, B. J. (1990). Shear induced order and shear processing of model hard sphere suspensions. *J. Rheol*, 34, 553–590

[20] Barnes, H.A. (1989). Shear-thickening (dilatancy) in suspensions of nonaggregating solid particles dispersed in Newtonian liquids. *J. Rheol*, 33, 329–366

[21] Barnes, H.A.; Hutton,J.F.; Walers, K.; (1989). *An Introduction to Rheology, Elsevier, Oxford.*

[22] Starov, V.; Zhdanov, V.; Meireles M. et al. (2002) Viscosity of concentrated suspensions: influence of cluster formation. *Advances in Colloid and Interface Science* , 96, 279-293

[23] Jaffe, B.; Cook, W. (1971). *Piezoelectric Ceramics*. Academic Press,London/New York.

[24] Damjanovic, D. (1998). Ferroelectric, dielectric and piezoelectric properties of ferroelectric thin films and ceramics. Reports on Progress in Physics,61, 1267.

[25] West, A. R.; Sinclair, D. C. and Hirose, N. (1997). *J. Electroceram*, 65, 71

[26] Cao, W. Q.; and Gerhardt, R. (1990). *Solid State Ionics*, 42, 213

[27] Barranco, A. P.; Pinar, F. C.; Martinez, O. P. ; Guerra, J. D. ; and Carmenate,I. G. (1999). *J. Eur. Ceram. Soc*, 19, 2677

[28] Raymond, M. V.; Smyth, D. M. (1996). Defects and charge transport in perovskite ferroelectrics. *J. Phys. Chem. Solids*, 57, 1507-1511

[29] Warren, W.L.; Pike, G.E.; Vanheusden,K.; Dimos, D.; Tuttle, B. A.; Robertson,J. (1996). Defect-dipole alignment and tetragonal strain in ferroelectrics. *J. Appl. Phys*, 79, 9250-9257

[30] Lambeck, P. V.; Jonker,G. H. (1978). *Ferroelectrics*, 22, 729

[31] Soares, MR.; Senos, AMR.; Mantas, PQ. (2000). Phase coexistence region and dielectric properties of PZT ceramics. *J. Eur. Ceram. Soc*, 20, 321-334

[32] Hammer, M.; Monty, C.; Endriss, A. (1998). Correlation between surface texture and chemical composition in undoped, hard, and soft piezoelectric PZT ceramics. *Journal of the American Ceramic Society*, 81, 721-724

[33] Xu, ZH.; Ducker, W.; Israelachvili, J. (1996). *Langmuir*, 12, 2263-2270

[34] Tomasik, P.; Schilling, CH.; Jankowiak, R.; Kim, JC. (2003). The role of organic dispersants in aqueous alumina suspensions. *Journal of the European Ceramic Society*, 23, 913-919

[35] Scott, J. F. (2007). *Science*, 315, 954-959

[36] Ma, LG.; Huang, Y.; Yang, JL.; Le, HR.; Sun, Y. (2006). Control of the inner stresses in ceramic green bodies formed by gelcasting. *Ceramics International*, 32, 93-98

[37] Barati, A.; Kokabi, M.; Famili, N. (2003). Modeling of liquid desiccant drying method for gelcast ceramic parts. *Ceramics International*, 29, 199-207

[38] Zheng, ZP.; Zhou, DX.; Gong, SP. (2008). Studies of drying and sintering characteristics of gelcast $BaTiO_3$-based ceramic parts. *Ceramics International*, 34, 551-555

[39] Wan, Yayun.; Ebbini, Emad S. (2008). Transactions on Ultrasonics Ferroelectrics and frequency Control. *IEEE* 55, 1705-1718

[40] Davies, BL.; Chauhan, S.; Lowe, M. (1998). International Conference on Medical Image Computing and Computer-Assisted Intervention. *Lecture Notesin Computer Science*, 1496, 386-396

[41] Saletes, Izella.; Gilles, Bruno.; Bera, Jean-Christophe. (2011). Promoting inertial cavitation by nonlinear frequency mixing in a bifrequency focused ultrasound beam. *Ultrasonics*,51, 94-101

[42] Li, XF.; Peng, XL.; Lee, KY. (2010). The static response of functionally graded radially polarized piezoelectric spherical shells as sensors and actuators. *Smart Materials & Structures*, 19, 3

[43] Guo, D.; Li, LT.; Cai, K.; Gui, ZL.; Nan, CW. (2004). Rapid Prototyping of Piezoelectric Ceramics via Selective Laser Sintering and Gelcasting. *Journal of the American Ceramic Society*, 87, 17-22

[44] Guo, D.; Cai, K.; Huang, Y.; Li, LT. (2003). A novel anti-spatter and anti-crack laser drilling technique: application to ceramics. *Applied Physics A:materials Science & Processing* , 76, 1121-1124

IntechOpen